N88-11160

COOLANT PASSAGE HEAT TRANSFER WITH ROTATION[1]

T.J. Hajek and A.W. Higgins

United Technologies Corporation
Pratt & Whitney

INTRODUCTION

In current and advanced gas turbine engines, increased speeds, pressures and temperatures are used to reduce specific fuel consumption and increase thrust/weight ratios. Hence, the turbine airfoils are subjected to increased heat loads escalating the cooling requirements to satisfy life goals. The efficient use of cooling air requires that the details of local geometry and flow conditions be adequately modeled to predict local heat loads and the corresponding heat transfer coefficients.

Improved turbine airfoil local temperature and hence, life predictions can be realized by accurately accounting for the effects of rotation on internal cooling. Although the effects of rotation which give rise to Coriolis and buoyancy forces can be large, they are currently not adequately included in the heat transfer designs of blades. Experimental data is particularly needed for the higher Rayleigh and Reynolds number conditions that are characteristic of turbine airfoil cooling passages. This data is crucial for development of design correlations and computer codes as well as their verification. Accurate prediction of local heat transfer coefficients enables the designer to optimize cooling configurations to minimize both metal temperature levels and thermal gradients. Consequently, blade life and engine efficiency can be significantly improved.

OBJECTIVE

The objective of this 36-month experimental and analytical program is to develop a heat tranfer and pressure drop data base, computational fluid dynamic techniques and correlations for multi-pass rotating coolant passages with and without flow turbulators. The experimental effort is focused on the simulation of configurations and conditions expected in the blades of advanced aircraft high pressure turbines. With the use of this data base, the effects of Coriolis and buoyancy forces on the coolant side flow can be included in the design of turbine blades.

EXPERIMENTAL MODEL

The coolant passage heat transfer model features a four-pass serpentine arrangement designed to reflect the passages within a gas turbine blade. Figure 1 shows a schematic diagram of the model with the instrumentation and wall sections indicated. Heat transfer coefficients are obtained for each wall section element. These wall elements, numbered 1 to 64, consist of a copper block backed with a thin film electrical resistance type heater and instrumented with two thermocouples. The copper wall sections are 10.7 mm x 49.3 mm (0.42 in. x 1.94 in.). Each section is thermally isolated from the adjoining section by a 1.5 mm (o.060 in.) thick divider strip of low thermal conductivity G-11 composite material. The straight radial passages have a square cross section, 12.7 mm x 12.7 mm (0.5 in. x 0.5 in).

1 NASA Contract NAS3-23691

DATA REDUCTION

Data acquisition/analysis consists of three general categories: equipment calibration, model heat loss measurement, and heat transfer coefficient calculations. The equipment calibration follows standard experimental procedures. Model heat loss measurements precede each test. These measurements are executed with no coolant flow and uniform wall temperature steady-state conditions; identical to the subsequent test less the coolant flow. Heat transfer coefficients are then calculated for each wall section element by applying the following procedure.

For each copper element the net energy convected to the fluid is calculated by subtracting the electrical line losses and conducted heat losses from the total energy supplied. Bulk fluid temperatures are then calculated based on an energy balance for each flowpath section as follows:

$$T_{b_{out}} = \frac{q_{net,\ 4\ walls}}{mc_p} + T_{b_{in}}$$

where the model inlet bulk temperature is measured. Once bulk fluid tempertures are determined, heat transfer coefficients are calculated from the equation:

$$h = \frac{q_{net,\ wall}}{A\ (T_w - T_b)}$$

where T_b is the average of the inlet and exit bulk temperatures. Thus for each test case, 64 heat transfer coefficients are calculated.

Table I shows the test conditions for which data were acquired with the smooth wall model. A total of 39 tests has been conducted to isolate the effects on heat transfer of rotation rate, flow rate, coolant-to-wall temperature variations, radius length and passage angle.

RESULTS

All of the heat transfer measurements for test conditions depicted in Table I were completed. Figures 2 and 3 show typical results for two tests conducted at the same Reynolds number but at different rotation rates. The data is plotted as the ratio of rotating to stationary heat transfer versus the streamwise position in the model. Figure 2 shows the leading and trailing walls of the passage, while Figure 3 depicts the sidewall results. As can be seen, the rotation significantly affects the heat transfer rates throughout the entire model. Augmentation factors of 300% as well as local reductions to 30% of stationary heat transfer rate values were encountered in the straight passages. Furthermore, heat transfer rates up to 5 times greater than the fully developed turbulent duct levels were seen to exist in the tip turns.

Due to the large number of data points obtained to date, comprehensive discussion of all the results is beyond the scope of this paper. Instead, the following paragraphs will focus on the first straight passage of the model. Detailed discussion of the heat transfer results along the leading and trailing surfaces of this radially outflowing leg will facilitate better understanding of the underlying physical principles.

Rotation of coolant passages introduces two forces not seen in stationary flows: Coriolis and centripetal. The Coriolis force has two major effects on internal flows. Firstly, it generates secondary flow circulations which cause the migration of low momentum sidewall fluid to the low pressure side of the channel. Secondly, it stabilizes/destabilizes the shear layer on the low/high pressure side of the passage. In the case of radially outward flow, the leading wall corresponds with the low pressure side of the passage and the trailing wall becomes the high pressure side. This trend reverses itself for radially inward flow.

Effect of Rotation

The high pressure side of the passage experiences a destabilization of the wall shear layers and cooler mainstream fluid will accelerate towards this wall. Increasing rotation rates will cause significant increases in heat transfer as seen in figure 4. Heat transfer rates can increase as much as 3 times the fully developed turbulent level for rotation number of Ro = 0.48.

The low pressure side of the passage is where the heated low energy fluid from the sidewalls is dumped. In addition to the fact that this already heated, relatively quiescent fluid tends to accumulate in this region, the rotation stabilizes the shear layers along this wall and further reduces the potential for heat removal. As a result, significantly lower than expected heat transfer rates were measured along the low pressure wall in a certain range of operating conditions. This result is quantified in figure 5, where the heat transfer rate is seen to drop to 40% of the fully developed level at Ro = 0.24. Heat transfer variations of this magnitude would generally affect the local blade metal temperature and thus airfoil lives.

Effect of Density Ratio

In general, increasing the wall temperature causes heat transfer rates to increase on both the low pressure and high pressure side of the passage for radially outward flow. Figure 6 shows the effects of $\Delta\rho/\rho$ variations for the leading and trailing surfaces. This is believed to be a centripetal buoyancy phenomenon, whereby centripetal buoyancy forces cause the heated wall layers to oppose the mainstream flow direction. An increased turbulence level in the wall shear layer generated by these opposing forces would account for the exhibited increase in heat transfer.

Effect of Radius

Figure 7 isolates the effect of distance from the axis of rotation on heat transfer. For the first two element sections (x/D = 1.5 and x/D = 4.6), the heat transfer on both the leading and trailing surfaces are essentially unaffected. Moving downstream inside the passage, the heat transfer decreases on both surfaces with the smaller radius. This is most likely a result of the weakening of the centripetal buoyancy forces at the smaller radius.

Laminarization on the Low Pressure Surface

As mentioned previously, the large decreases in heat transfer seen on the low pressure side of the passage should be of utmost concern to turbine blade designers. The remainder of this paper will examine the cause of this deficiency. Specifically, the low pressure surface (in all three straight passages) or the leading surface in the first passage, is believed to laminarize for certain ranges of rotation rates and

density ratios. Outside of these ranges the wall shear layers become transitional and heat transfer increases.

The isolated effect of rotation number for Reynolds number of Re = 25,000 is depicted in figure 5. As the rotation number increases large decreases in heat transfer occur. This minimum level attained changes in both magnitude and position with variations in the rotation number.

Figure 8 plots all the leading side data for ΔT = 80°F and Re = 25,000. The data is plotted as Nu_x, x being the distance from the inlet, versus a rotational Raleigh number

$$Ra_x = \left(\frac{\Omega^2 R \; x^3 \; \Delta T}{\nu^2 \; T_b} \right) Pr$$

Note for each line of constant Ro there are three data points. Each of these correspond to one of the three test section elements downstream of the guard heaters at the inlet: elements 34, 35, and 36 in figure 1.

For the higher rotation rates, Ro > 0.18, the heat transfer, plotted as Nu_x, tends to collapse on a single curve. This curve attains a minimum around Nu_x = 200 and begins a sharp upturn at $Ra_x = 10^{11}$. Based on the results to date, it is believed that for the lower rotation rates the data is predominantly governed by Coriolis forces while at the highest rates centripetal buoyancy dominates. There is a flow regime between these two extremes where the wall shear layer is believed to be laminar. This hypothesis is supported by the following figures.

Figure 9 plots Nu_x versus Ra_x, for high rotation, Ro > 0.18, and it includes all four temperature cases (figure 3 included only ΔT = 80). Two important points should be emphasized. Firstly, for $10^{10} < Ra_x < 10^{11}$ the heat transfer is constant at Nu_x = 210. This level defines the minimum heat transfer attained for Re = 25,000. Secondly, for $Ra_x > 10^{11}$, Nu_x increases significantly. This increase for large Ra_x is believed to be induced by centripetal buoyancy forces.

Consider the range of data where the heat transfer is constant at Nu_x = 210 (fig. 9). If this data is compared to both the fully turbulent stationary heat transfer and to Kays (ref. 1) analytical solution for laminar flat plate heat transfer: $Nu_x = 0.565 \; Pr^{1/2} \; Re_x^{1/2}$ (figure 10), it appears to be nearly indentical to the laminar correlation, thus supporting the hypothesis that a flow regime containing laminar shear layer does exist.

These results can be further sustantiated by examining the work of J. P. Johnston (ref. 2). In his rotating channel experiment at Stanford University, he discovered regions where the boundary layer on the leading wall was laminar for Reynolds numbers as high as Re = 15,000. Figure 11 schematically depicts the important characteristics
of this flowfield.

On the leading side of the 7:1 aspect ratio channel, Johnston saw a nearly parabolic mean velocity profile and an absence of the bursting process normally seen at the wall in turbulent flow. On the other side of the channel, Taylor-Goertler type roll cells developed within the turbulent section of the mean velocity profile. The laminar boundary layer on the leading surface and the highly turbulent boundary

layer with bursting roll cells on the trailing surface help explain the large decreases and increases seen in heat transfer with rotation.

One of Johnston's conclusions was that the rotation induced re-laminarization was highly Reynolds number dependent. To evaluate this dependency, the present NASA data was examined at varying Reynolds numbers.

Figures 12 and 13 compare the rotating heat transfer results at Re = 12,500 and Re = 50,000, respectively, to Kays correlation for laminar flow. The lower Reynolds number flow case, figure 12, matches Kays correlation at test sections 34 and 35, while the higher Reynolds number flow never reaches the laminar level; although it approaches this minimum. This data indicates that for high rotation rates the boundary layer on the leading wall is more likely to be laminar at low Reynolds number. This work compares very well with Johnston's results.

Johnston used flow visualization techniques to establish when the leading wall would laminarize. Figure 14 extends Johnston's mapping of flow regimes with rotation. The NASA data at three different Reynolds numbers is shown to complement Johnston's results. At the low Reynolds number the leading side is laminar for Ro = 0.24. At the high Reynolds number the shear layer is most likely transitional; somewhere close to but not yet laminar. At the middle Reynolds number flow, Re = 25,000, there exists extensive data to clarify where the flow becomes laminar. Remember this region existed when $Nu_x = 210$. This is when $10^{10} < Ra_x < 10^{11}$, indicating that buoyancy plays an important role in the laminarization process.

Two important results need to be highlighted:

1. The minimum level of heat transfer attained is predicted by Kays laminar flat plate correlation.

2. Centripetal buoyancy limits this laminarization process. For Re = 25,000 and $Ra_x > 10^{11}$ the leading side shear layer becomes transitional and the heat transfer increases.

WORK PLANNED

Currently the model is being modified to include turbulators on the leading and trailing surfaces of the straight radial passages. Two experimental programs are planned; one with turbulators aligned at an angle of 45° and one with turbulators normal to the axis of the passage. This testing will examine the effects of rotation on highly enhanced heat transfer coolant passages.

<u>Dimensional Parameters</u>

Reynolds number, Re	$\rho V d_H/\mu = V d_H/\nu = m d_H/(A\ )$
Rotation number, Ro	$\Omega d_H/V$
Density or Temperature ratio	$\Delta\rho/\rho$, $\Delta T/T$
Radius ratio	R/d_H
Rotational Grashof number, Gr	$Ro^2 Re^2 (\Delta T/T)(R/d_H)$
Nusselt number, Nu	$h d_H/k$

REFERENCES

1. W.M. Kays and M.E. Crawford, Convective Heat and Mass Transfer, Second Edition, McGraw-Hill Book Company, 1980.

2. J.P. Johnston, "The Effects of Rotation on Boundary Layer in Turbomachine Rotors", Report MD-24, Thermosciences Division, Mechanical Engineering Dept., Stanford University, May 1970.

TABLE I

TEST CONDITIONS FOR ROTATING HEAT TRANSFER EXPERIMENTS WITH SMOOTH WALL MODEL
Contract NAS3-23691

Test No.	Basic Dimensionless Parameters						Secondary Dimensionless Parameters		
	α (deg)	Re	Ro	$\frac{\Delta T}{T_{IN}}$	$\frac{\bar{R}}{d_H}$	$\frac{\Delta\rho}{\rho}$ $\frac{\Omega R}{V}$	Gr/Re^2	$Gr \times 10^{-8}$	Comments
1	--	25,092	0	0.	--	0	0	0	
2	--	12,490	0	0.14	--	0	0	0	Nonrotating
3	--	49,985	0	0.14	--	0	0	0	
4	0	25,221	0.238	0.15	49	1.29	0.22	1.96	Baseline
5	0	12,591	0.227	0.15	49	1.18	0.19	0.43	
6	0	49,627	0.253	0.15	49	1.41	0.25	8.81	Re Varied
7	0	24,475	0.475	0.15	49	2.46	0.82	7.33	
8	0	24,812	0.118	0.15	49	0.64	0.05	0.46	Ro Varied
9	0	25,299	0.244	0.07	49	0.72	0.72	1.13	
10	0	25,117	0.237	0.23	49	1.82	0.30	2.73	$\Delta T/T$ Varied
101	0	25,035	0.006	0.15	49	0.04	0.00	0.00	Low Ro effects on leading wall
102	0	24,242	0.233	0.30	49	2.22	0.36	3.06	Additional point at max ΔT
103	0	75,295	0.116	0.15	49	0.64	0.05	4.20	Effect of Re
104	0	50,033	0.119	0.15	49	0.66	0.06	1.98	at Ro = 0.11
105	0	25,166	0.362	0.07	49	1.04	0.28	2.39	
106	0	24,730	0.350	0.15	49	1.84	0.45	4.22	Effect of ΔT
107	0	24,914	0.350	0.22	49	2.61	0.64	5.70	at Ro = 0.35
108	0	25,039	0.006	0.15	49	0.04	0.0	0.00	Symmetry
109	0	24,955	0.233	0.15	49	1.23	0.20	1.79	check
110	0	25,098	0.000	0.07	49	0.00	0.00	0.00	Effect of ΔT
111	0	25,098	0.000	0.23	49	0.00	0.00	0.00	at Ro = 0.0
112	0	25,082	0.000	0.31	49	0.00	0.00	0.00	
113	0	25,076	0.178	0.23	49	1.38	0.17	1.55	Effect of ΔT
114	0	24,840	0.178	0.15	49	0.97	0.12	1.06	at Ro = 0.18
115	0	25,131	0.183	0.08	49	0.54	0.07	0.63	
116	0	25,021	0.171	0.31	49	1.66	0.20	0.18	
117	0	25,018	0.062	0.15	49	0.34	0.01	0.13	Effect of R_O
12	45	24,805	0.24	0.15	49	1.32	0.22	1.98	Effect of a
118	45	24,627	0.23	0.23	49	1.77	0.29	2.52	change; varing
119	45	24,670	0.34	0.15	49	1.76	0.42	3.66	ΔT and Ro at
120	45	24,605	0.32	0.12	49	2.28	0.51	4.48	Re = 25,000.
121	45	24,778	0.18	0.15	49	0.94	0.12	1.02	
122	45	24,745	0.17	0.22	49	1.26	0.15	1.30	
13	45	24,818	0.23	0.14	49	1.20	0.19	1.71	Reversal of
123	45	24,907	0.22	0.22	49	1.60	0.24	2.18	Rotation Direction for a change.
11	0	24,863	0.24	0.15	33	0.87	0.15	1.31	
124	0	24,858	0.22	0.31	33	1.42	0.24	1.99	Radius Change
125	0	24,774	0.35	0.15	33	1.19	0.31	2.57	Effects on
126	0	24,886	0.33	0.33	33	2.02	0.47	4.18	Centrifugal Buoyancy Parameter Gr/Re^2

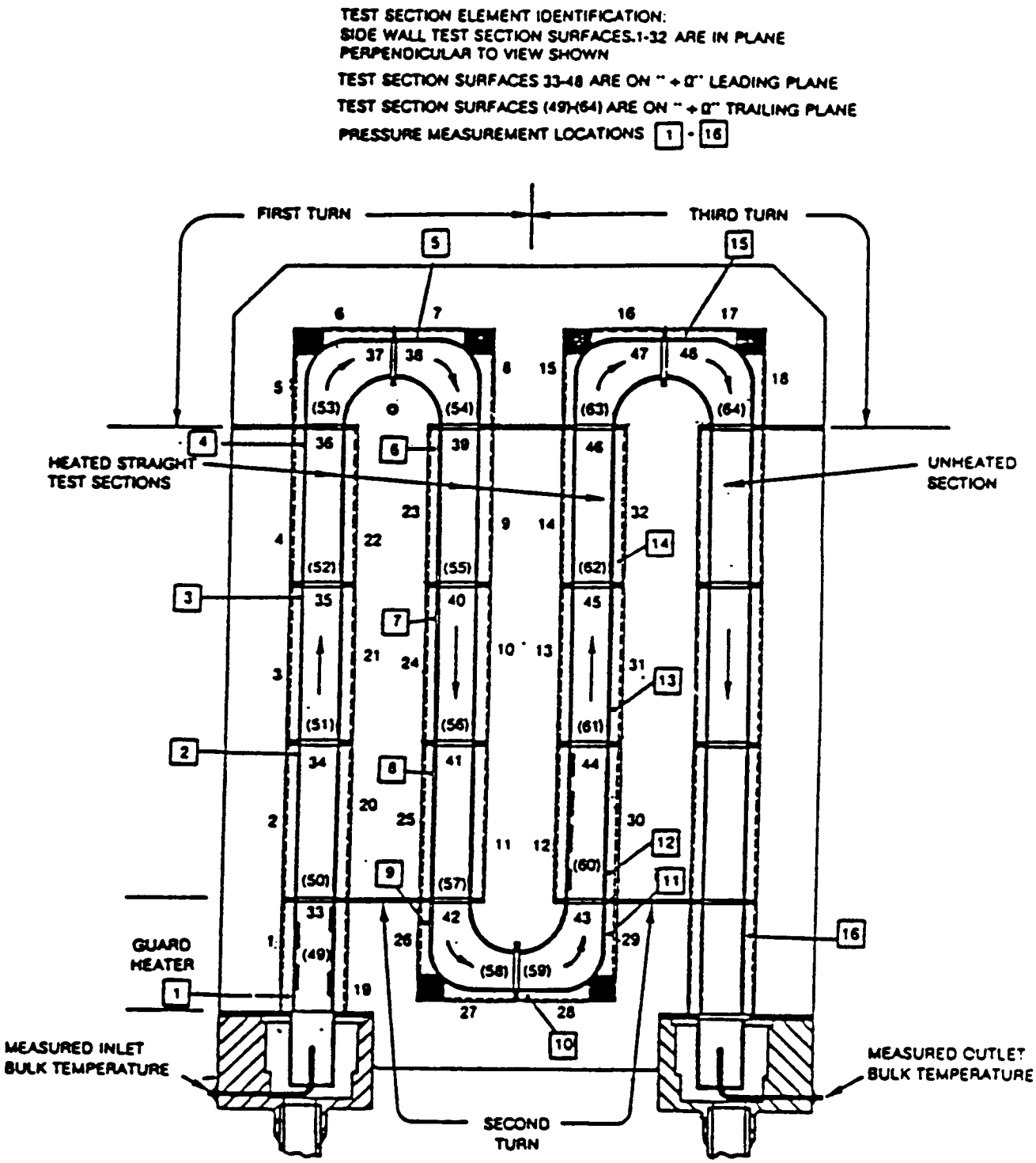

Figure 1 Instrumentation Plan for Coolant Passage Heat Transfer Model

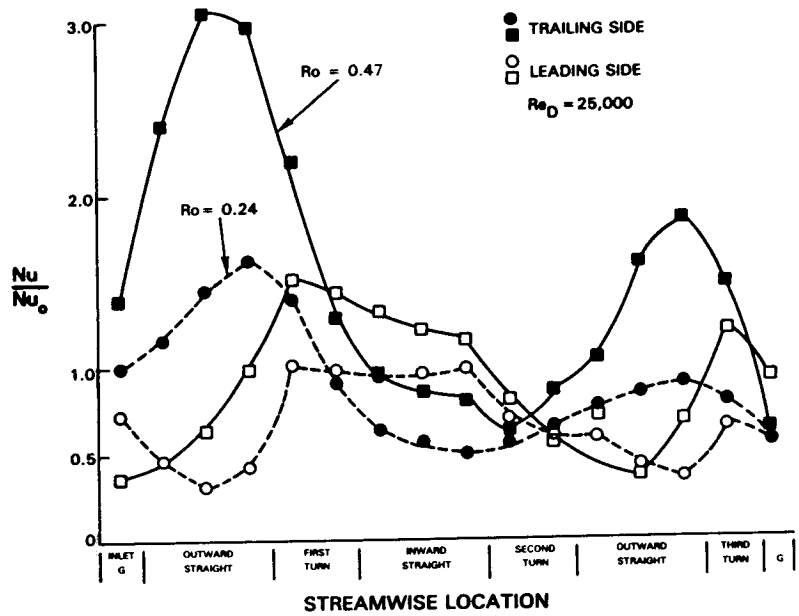

Figure 2 Leading and Trailing Surface Heat Transfer; Test Nos. 7 & 9

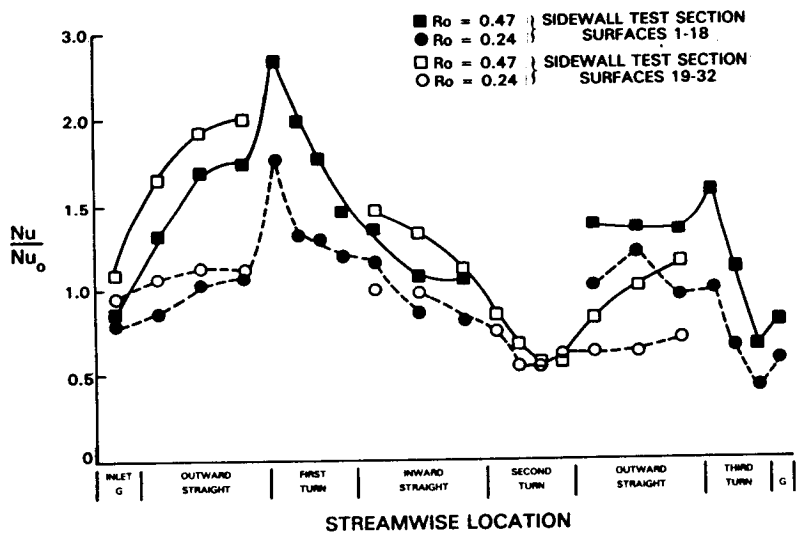

Figure 3 Sidewall Heat Transfer; Test Nos. 7 & 9

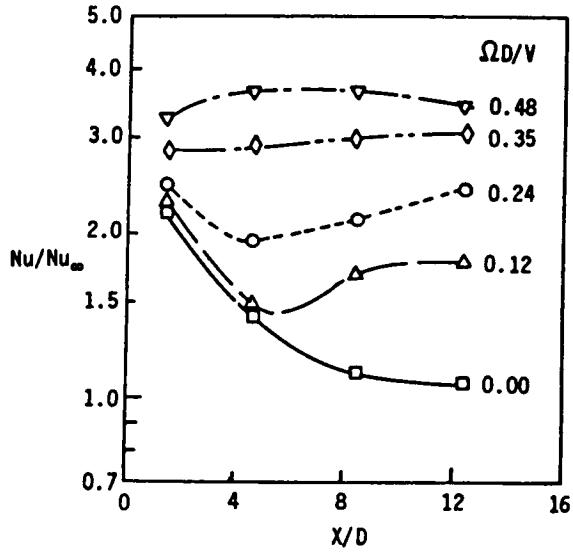

Figure 4 Effect of Rotation Number on Trailing Surface Heat Transfer
Re = 25,000, $\Delta\rho/\rho$ = 0.11, $\bar{R}/D$ = 49

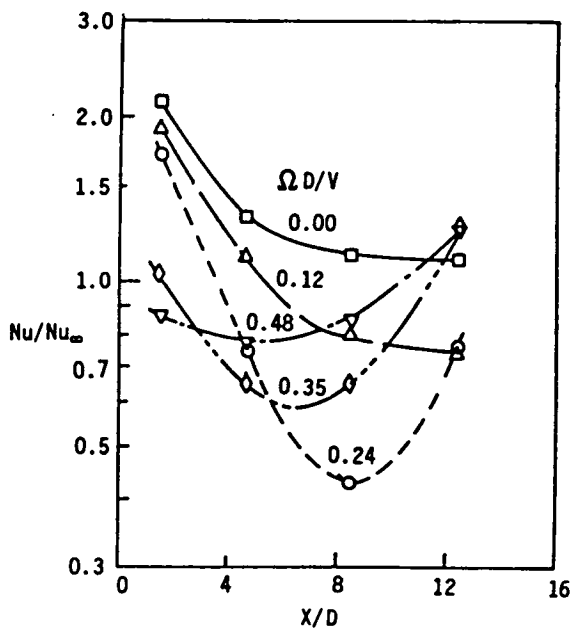

Figure 5 Effect of Rotation Number on Leading Surface Heat Transfer Ratio
Re = 25,000, $\Delta\rho/\rho$ = 0.11, $\bar{R}/D$ = 49

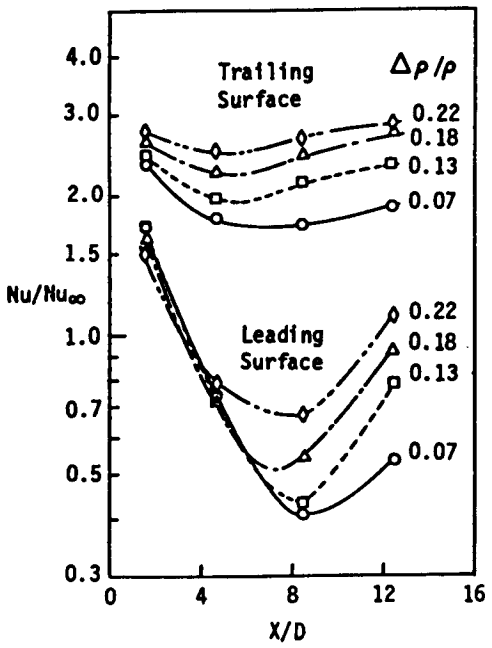

Figure 6 Effect of Wall to Bulk Density Difference Re = 25,000, $\Omega D/V = 0.24$, $\bar{R}/D = 49$

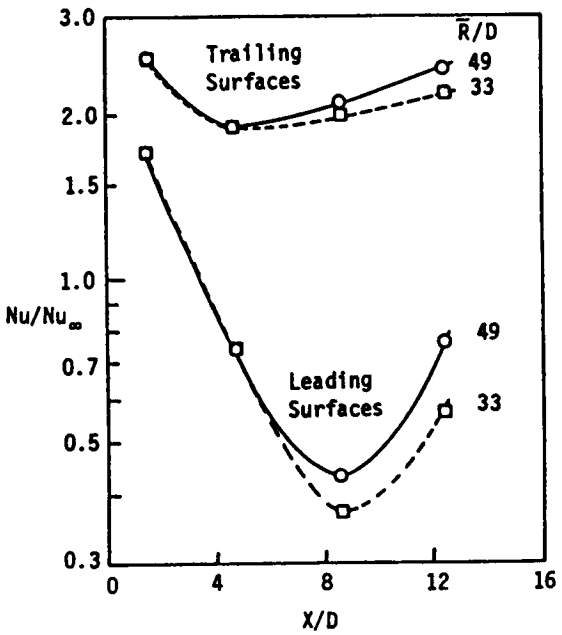

Figure 7 Effect of Model Radius on Heat Transfer Ratio Distribution; Re = 25,000, $\Omega D/V = 0.24$, $\Delta\rho/\rho = 0.13$

LOW PRESSURE SIDE OF PASSAGE Re ≈ 25,000

SYMBOL	○	◊	×	△	∩	□	◿	▽	SYMBOL FLAGS
ROTATION NUMBER	0.0	0.006	0.06	0.12	0.18	0.25	0.35	0.50	
TEST NO. AT ΔT = 40°F	110	–	–	–	115	9	105	–	
ΔT = 80°F	1	101	117	8	114	4	106	7	
ΔT = 120°F	111	–	–	–	113	10	107	–	
ΔT = 160°F	112	–	–	–	116	102	–	–	

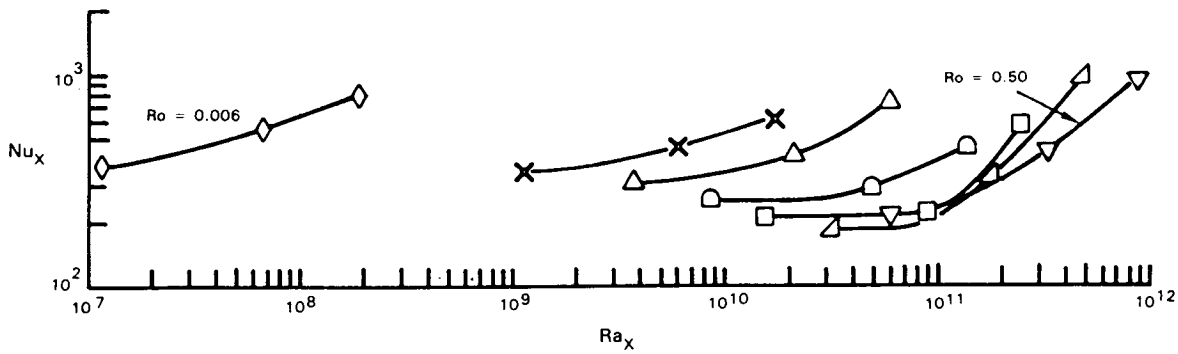

Figure 8 Leading Side Heat Transfer for 1st Passage; Radially Outward Flow

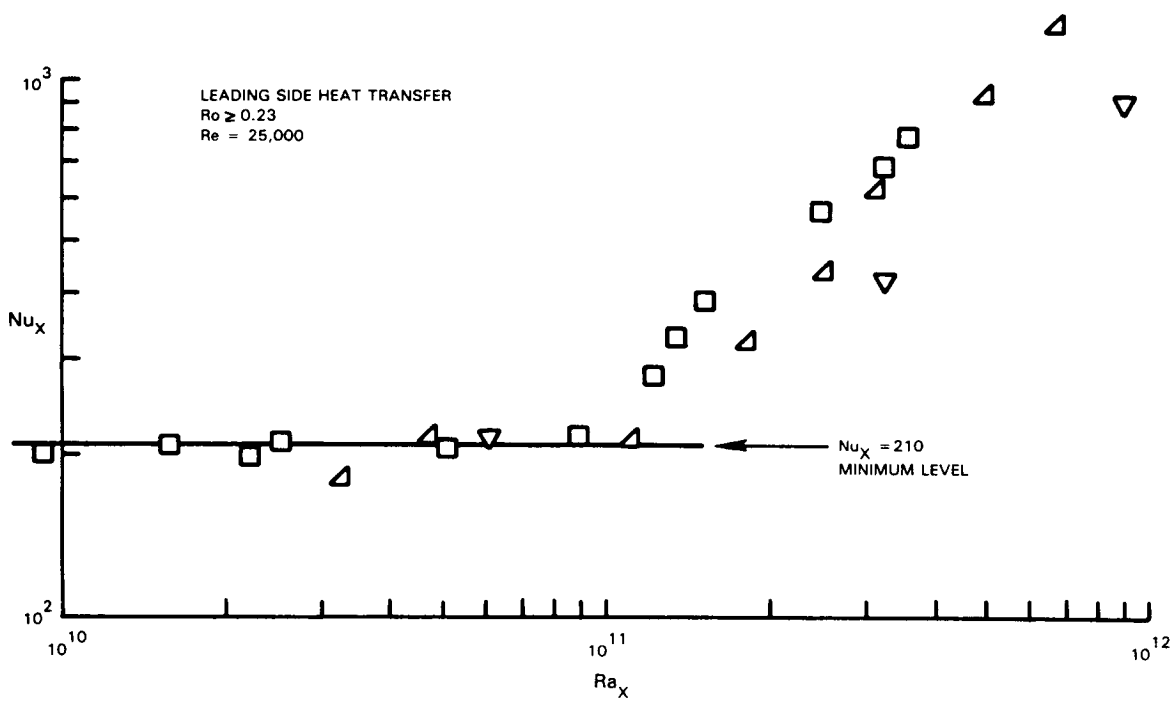

Figure 9 Leading Side Heat Transfer Ro ≥ 0.23: Re = 25,000

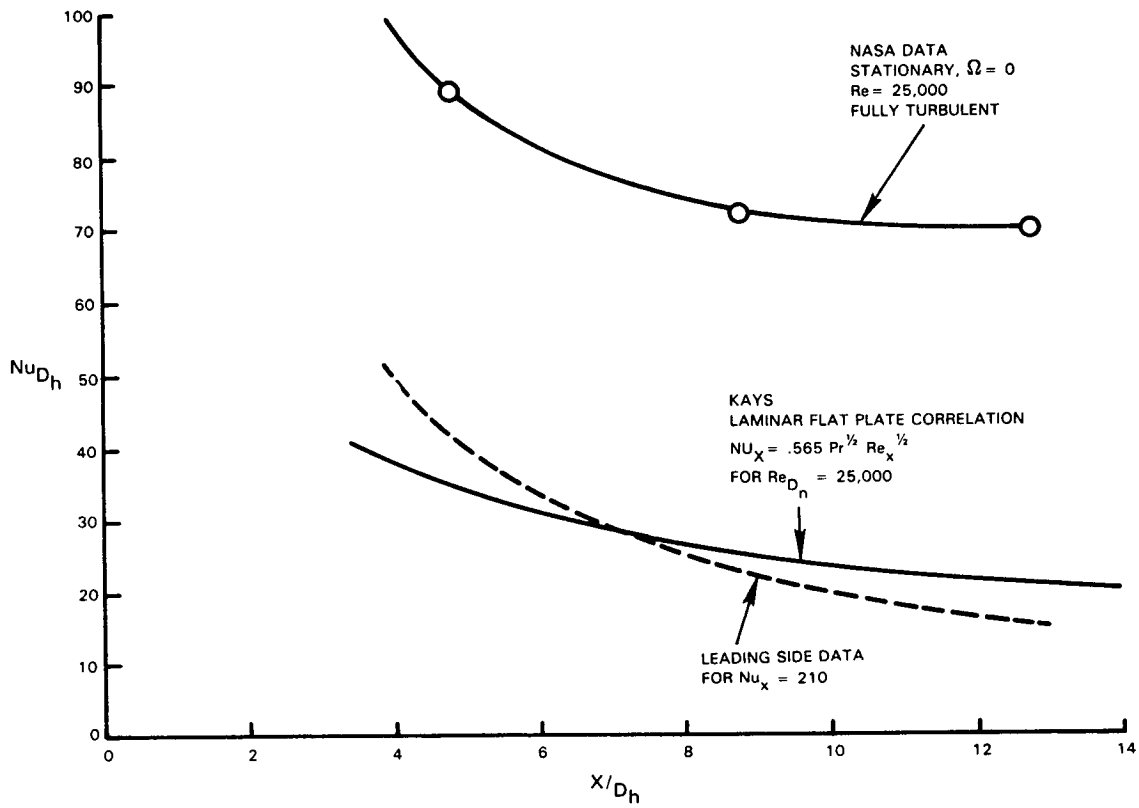

Figure 10 Leading Side Heat Transfer with Rotation Compared to Kays Laminar Heat Transfer: Re = 25,000

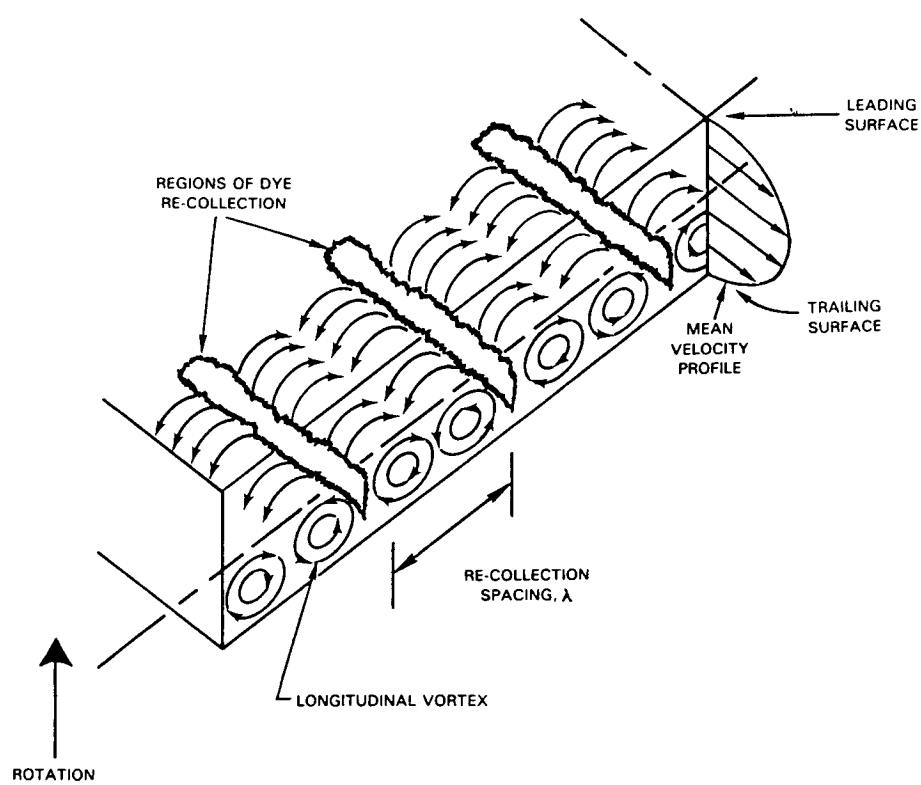

Figure 11 J. P. Johnston Flow Visualization of Rotating Channel Flow

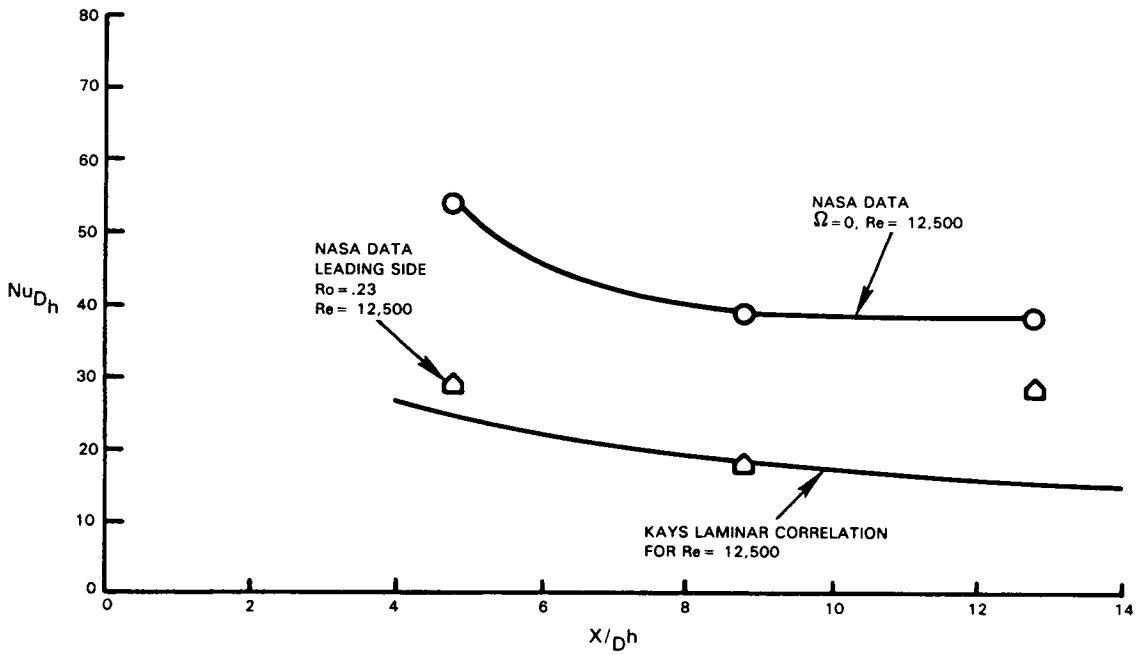

Figure 12 Leading Side Heat Transfer with Rotation Compared to Kays Laminar Heat Transfer: Re = 12,500

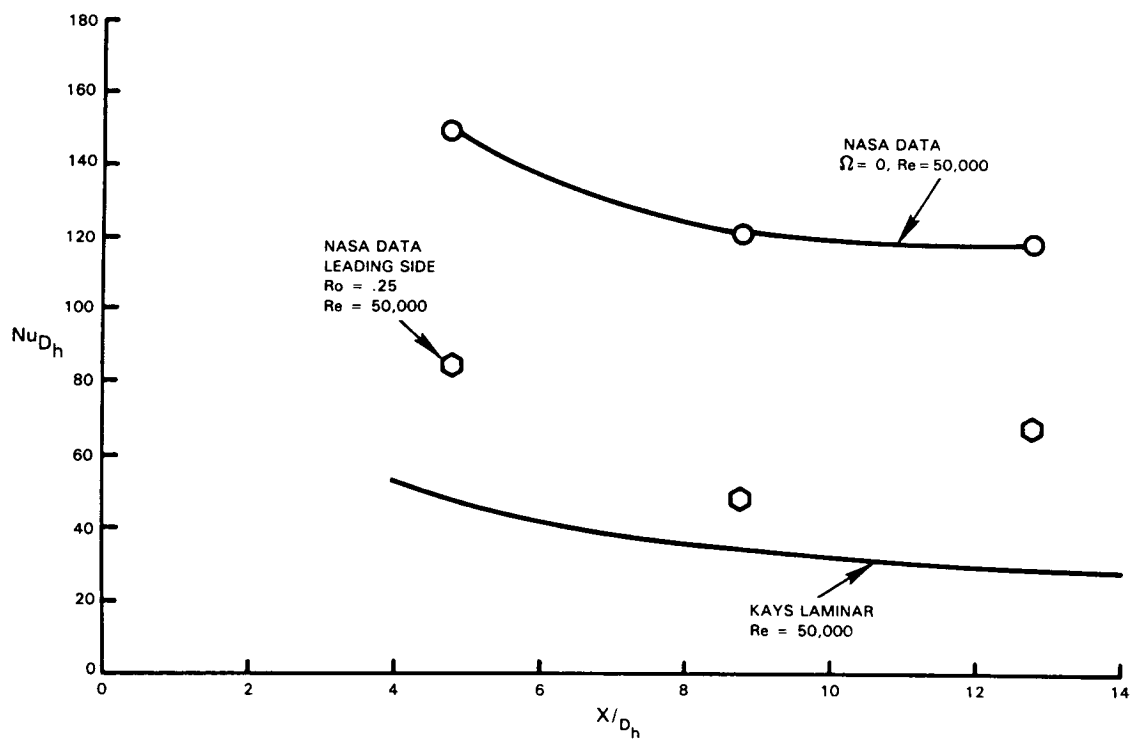

Figure 13 Leading Side Heat Transfer with Rotation Compared to Kays Laminar Heat Transfer: Re_D = 50,000

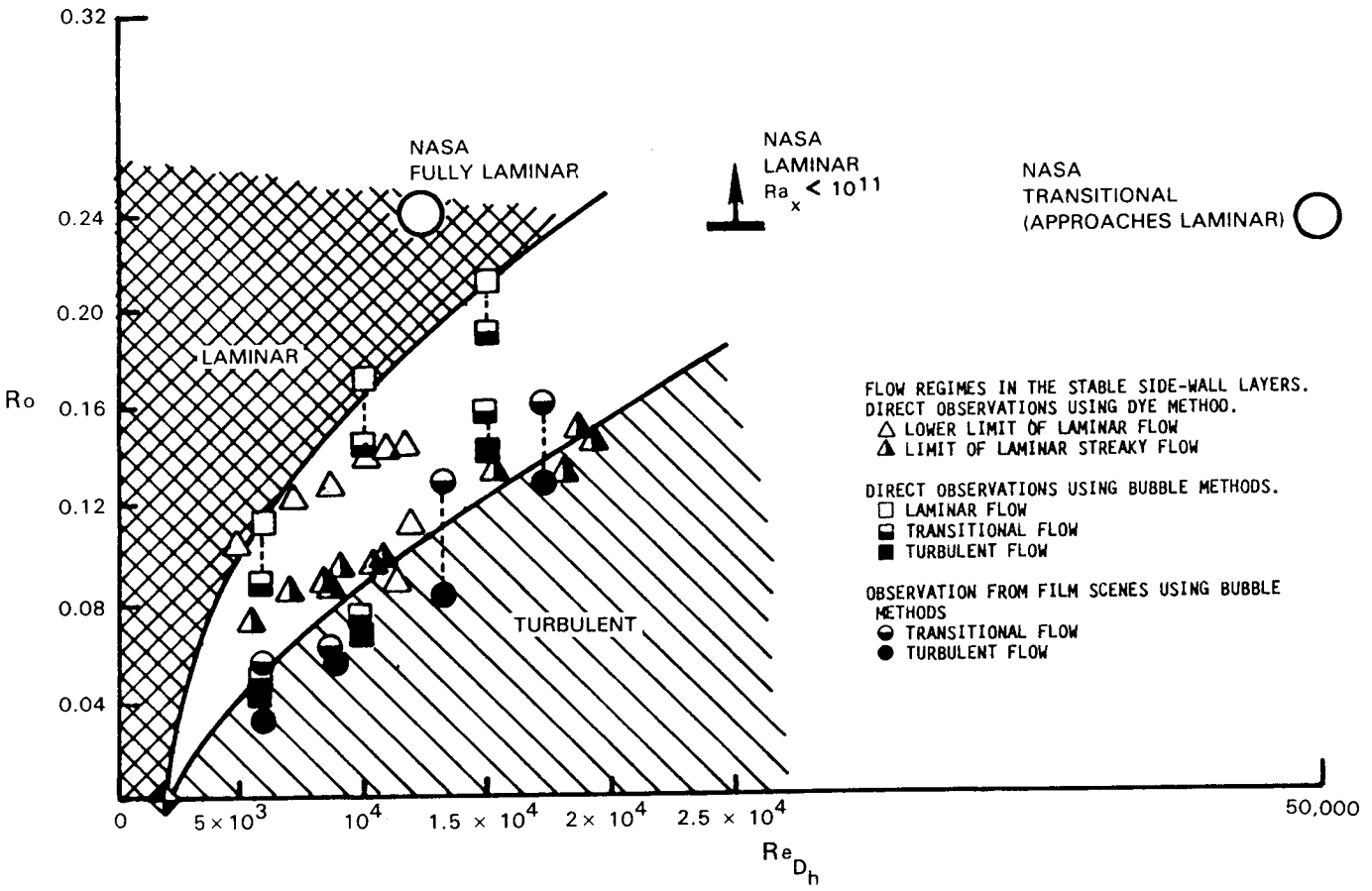

Fgiure 14 NASA Data Plotted on Johnston's Flow Map